ACSNANO
www.acsnano.org
ARTICLE

Improving Contact Interfaces in Fully Printed Carbon Nanotube Thin-Film Transistors

Changyong Cao,[†] Joseph B. Andrews,[†] Abhinay Kumar,[†] and Aaron D. Franklin*[,†,‡]

[†]Department of Electrical and Computer Engineering, Duke University, Durham, North Carolina 27708, United States
[‡]Department of Chemistry, Duke University, Durham, North Carolina 27708, United States

Supporting Information

ABSTRACT: Single-walled carbon nanotubes (CNTs) printed into thin films have been shown to yield high mobility, thermal conductivity, mechanical flexibility, and chemical stability as semiconducting channels in field-effect, thin-film transistors (TFTs). Printed CNT-TFTs of many varieties have been studied; however, there has been limited effort toward improving overall CNT-TFT performance. In particular, contact resistance plays a dominant role in determining the performance and degree of variability in the TFTs, especially in fully printed devices where the contacts and channel are both printed. In this work, we have systematically investigated the contact resistance and overall performance of fully printed CNT-TFTs employing three different printed contact materials—Ag nanoparticles, Au nanoparticles, and metallic CNTs—each in the following distinct contact geometries: top, bottom, and double. The active channel for each device was printed from the dispersion of high-purity (>99%) semiconducting CNTs, and all printing was carried out using an aerosol jet printer. Hundreds of devices with different channel lengths (from 20 to 500 μm) were fabricated for extracting contact resistance and determining related contact effects. Printed bottom contacts are shown to be advantageous compared to the more common top contacts, regardless of contact material. Further, compared to single (top or bottom) contacts, double contacts offer a significant decrease (>35%) in contact resistance for all types of contact materials, with the metallic CNTs yielding the best overall performance. These findings underscore the impact of printed contact materials and structures when interfacing with CNT thin films, providing key guidance for the further development of printed nanomaterial electronics.

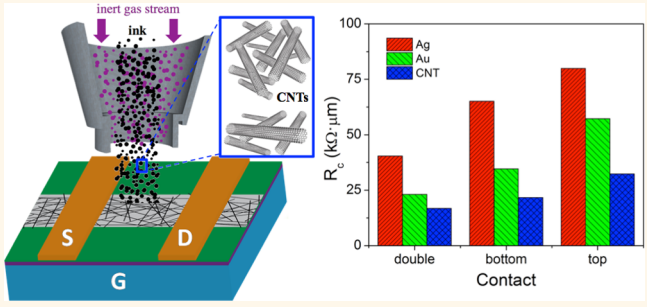

KEYWORDS: *thin-film transistor (TFT), contact resistance, carbon nanotube (CNT), aerosol jet printing, nanomaterials*

Advances in the synthesis and processing of nanomaterials, combined with their superb electrical properties, have led to their strong consideration for printed electronics. Single-walled carbon nanotubes (CNTs) have been intensely studied for use in thin-film transistors (TFTs) due to their high carrier mobility, excellent chemical stability and mechanical flexibility, as well as compatibility with solution-based processing.[1−8] Example applications that have been demonstrated using CNT-TFTs include simple logic circuits,[9] display backplanes,[10] sensors,[11] and radio frequency identification antennae.[12] A variety of applications in the realms of flexible electronics and Internet of Things (IoT) would be made possible with low-cost TFTs that have reasonable performance; printed CNT-TFTs have tremendous potential for providing such performance but have been hindered by obstacles that include material processing and contact resistance. During the past decade, the difficulty in achieving high-purity semiconducting CNTs during synthesis has led to extensive efforts in solution-processed purification, which allows CNTs to be rapidly and cheaply separated based on their electronic type.[13−16] Importantly, it has been shown that the structural defects induced during the solution-based purification and suspension processes for CNTs do not degrade the quality of the electrical contact formed between the nanotube and metal electrodes.[17,18] TFTs with record-breaking performance have been demonstrated using carbon nanotubes with semiconducting purity above 99% produced by a density-gradient ultracentrifugation method.[1,7,19]

One of the most promising aspects of CNT-TFTs is their compatibility with low-cost, high throughput printing processes. These include gravure printing, screen printing, and inkjet printing, each of which has been gaining increased attention in both industrial and academic sectors.[7,20−24] However, the printing resolutions of gravure printing and screen printing are relatively low, although they can be used for large area roll-to-roll printing. Inkjet printing is a very common and accessible form of printing but has the tendency of clogging in the inkjet

Received: February 3, 2016
Accepted: April 15, 2016

DOI: 10.1021/acsnano.6b00877
ACS Nano XXXX, XXX, XXX−XXX

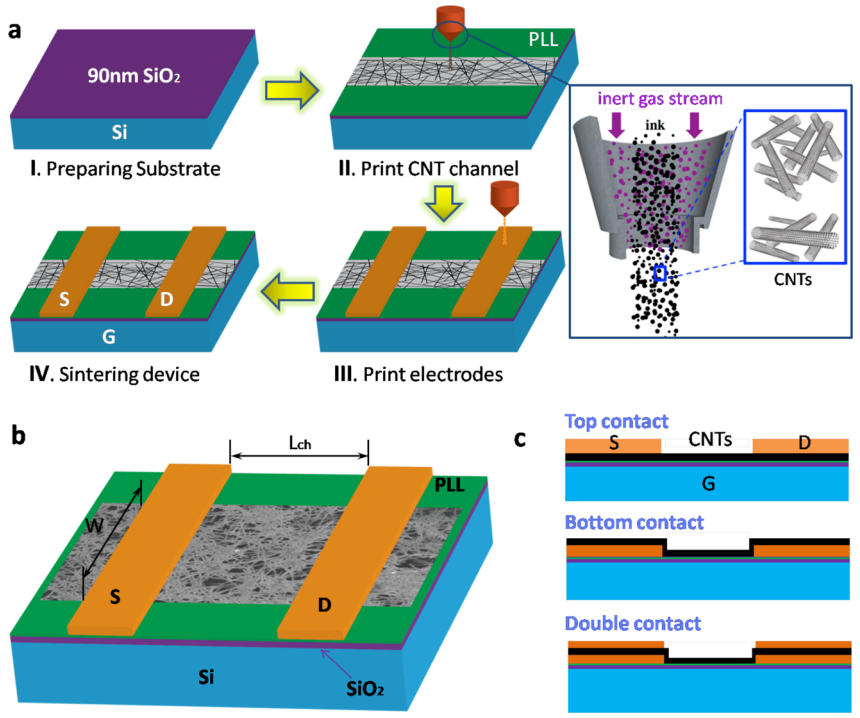

Figure 1. (a) Schematic fabrication process flow for printed, back-gated CNT-TFTs, including (I) preparing silicon wafer by first cleaning with acetone, IPA, DI water, and then oxygen plasma treatment; (II) modification of the SiO_2 with poly-L-lysine (PLL) followed by printing the CNT thin-film channel with an aerosol jet printer; (III) aerosol jet printing the source/drain electrodes; and (IV) sintering of the final device. The inset schematically shows a magnified, cross-sectional view of the aerosol jet print head where the aerosolized nanomaterial ink is guided out of the nozzle by a sheath of inert gas (N_2). (b) Schematic diagram of a printed, back-gated CNT-TFT with indication of key dimensions. (c) Schematic view of the three different contact configurations studied in this work: top, bottom, and double contacts.

heads during the printing of nanomaterials.[25−27] It is also challenging for inkjet printing to achieve high-resolution patterns due to the difficulty of controlling the size and shape of ink droplets. To improve the electrical performance, partially printed devices requiring some photolithography or electron beam lithography processes have often been used, but these lack practical application in the truly low cost, printed electronics space.[19,28]

A promising technique that has received limited attention for printing nanomaterials is aerosol jet printing,[19,28−31] which is a more refined version of inkjet printing. Rather than directly printing an ink solution through a nozzle, the ink is first aerosolized, either pneumatically or ultrasonically, in a stream of inert gas. This aerosol is then printed onto the substrate through a nozzle where it is further focused into a fine stream using a sheath of inert gas. The result is the ability to print lines down to ∼10 μm in width having significantly reduced drying/sintering times owing to the lowered presence of solvent from the aerosol process. Regardless of the printing process used, the carrier mobility (<0.1 $cm^2\ V^{-1}\ s^{-1}$) and operation voltage (>20 V) of most printed CNT-TFTs (with printed source/drain contacts) have been limited by the morphology of the printed layers, the purity of the semiconducting CNTs in the active channel film, and the substantial contact resistance. The contact resistance plays a particularly dominant role in determining the performance and degree of variability in the CNT-TFTs,[32,33] and thus requires further investigation.

In this study, we show that the contact resistance in fully printed CNT-TFTs can be lowered by >35% with minor alterations to the contact geometry. Further, three different metallic inks were investigated for their impact on contact resistance in different contact geometries including: top, bottom and double (a sandwich-like structure combining contacts below (bottom) and above (top) the printed CNTs). All of the CNT-TFTs in this work were printed using an aerosol jet printer. The three types of printed nanomaterial inks that were explored for source/drain contacts were silver (Ag) nanoparticles, gold (Au) nanoparticles. and metallic CNTs. Devices with different channel lengths (from 20 to 500 μm) were fabricated and tested for each contact geometry and metal to allow for the extraction of contact resistances using the transmission line method (TLM). It was found that, compared with single (top or bottom) contacts, double contacts offer a significant decrease in contact resistance for CNT-TFTs for all three of the electrode materials. It is also shown that the printed CNT transistors made completely from CNTs have the lowest contact resistance, indicating that the CNT-CNT contact performance is better than that of metal-CNT contacts when using print processing. These findings for the contact resistance of printed CNT-based transistors help minimize the impact of contacts on device performance and guide further optimization of printed nanomaterial electronics.

RESULTS AND DISCUSSION

The process used for fabricating the printed CNT-TFTs on a Si wafer with 90 nm thick SiO_2 is illustrated in Figure 1. The substrate was first cleaned with acetone, IPA and deionized (DI) water, followed by oxygen plasma (100 W) for 3 min. In the case of bottom- or double-contact structures (Figure 1c), the source and drain contacts were then printed using the parameters outlined for the specific inks in the Supporting Information. The surface was then functionalized by immersing

DOI: 10.1021/acsnano.6b00877
ACS Nano XXXX, XXX, XXX−XXX

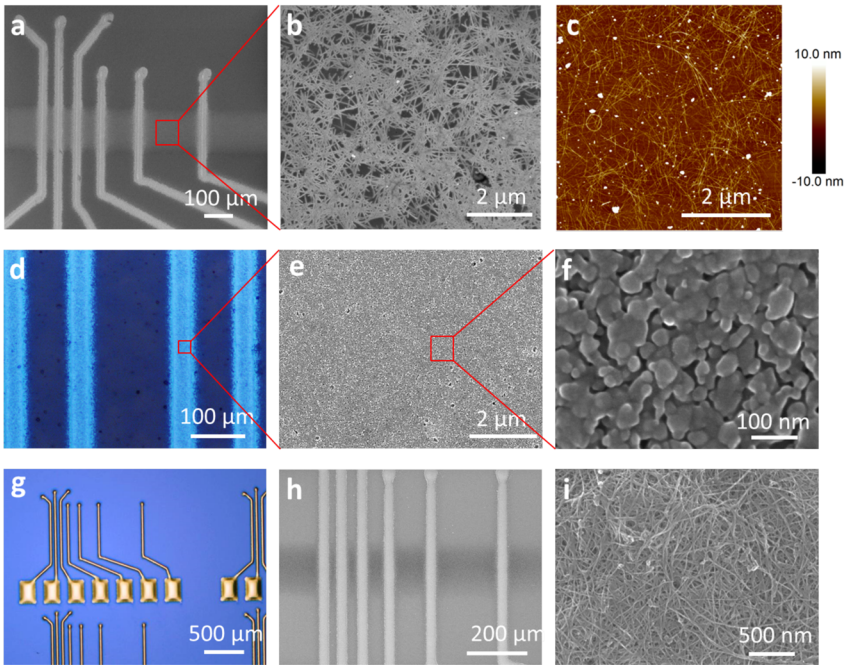

Figure 2. Morphology of as-printed, back-gated CNT-TFTs. (a) SEM image of representative back-gated CNT-TFTs with bottom silver (Ag) contact electrodes for various channel lengths. (b) SEM image of a printed CNT thin-film in the channel region. The CNT network is uniformly distributed and its density is ~45 CNTs/μm^2. (c) AFM image of the nanotube thin-film channel. (d) Optical image of as-printed Ag ink with a width of ~40 μm and thickness of ~0.6 μm showing good morphology. (e and f) SEM images of the printed Ag contact electrodes after sintering at 150 °C for 1 h. Note how Ag nanoparticles have been merged together leading to a much smaller resistance. (g and h) Optical and SEM images of the printed gold (Au) source/drain electrodes in CNT-TFTs. (i) SEM image of printed metallic CNT source/drain thin-films after 10 printing passes. Details on the relationship between resistance and number of passes are given in Supporting Information.

into poly-L-lysine (PLL) solution (0.1% w/v in water; Sigma-Aldrich) for 5 min to enhance CNT adhesion to the SiO_2.[7,34,35] Semiconducting CNT channels were printed onto the substrate using an aerosol jet printer. The semiconducting CNT ink was made from 99.9% semiconducting nanotubes (IsoNanotubes-S) obtained from NanoIntegris, Inc. To remove the surfactant involved in the CNT network, a brief rinse with toluene was performed after the printed CNT films had dried. At this point, the source and drain contacts for the top-contact geometry were printed. Also, printing of the top portion of the sandwich-like contact structure directly on top of the already established bottom portion completed the double contacts. For the Ag and Au contacts, commercial silver nanoparticle solution (Ag40X, UT Dots, Inc.) and gold nanoparticle solution (UTD-Au25, UT Dots, Inc.) were used, whereas for CNT contacts, single-walled metallic CNT powders (P3-SWNT, Carbon Solution, Inc.) were dispersed in DI water followed by 2 h ultrasonication to form a 0.5 mg/mL solution. A postprinting sintering step for the electrodes was performed to achieve better conductivity. In the double-contact design, the sintering step was performed each time after the bottom and top portions were printed.

All printing in this work was carried out using an aerosol jet printing system (Optomec, AJ-300). The aerosol jet process is a versatile method for patterning a wide range of electronically functional liquid inks, including precursor inks, nanoparticle suspensions, diluted electronic pastes, and biological materials.[36] Feature sizes down to 10 μm can be printed with high repeatability, good edge definition, high conductivity from high metal loading, single-pass thickness from 10 nm to 5 μm, low surface roughness, and strong adhesion with a variety of substrates. With the use of aerodynamic focusing, the printer allows for high-resolution deposition of colloidal suspensions and/or chemical precursor solutions. The aerosol stream with droplets of 1−5 μm in diameter is focused using a flow deposition head, which forms an annular, coaxial flow between the aerosol stream and a sheath gas stream. The coaxial flow exits the print head through a nozzle directed at the substrate. The printer has a dual camera system monitoring substrate alignment markers and the current printed layer to make fine adjustments to the stage position and rotation before each printing that ensures proper alignment between layers.

Details of the morphology of the as-printed, back-gated CNT-TFTs are shown in Figure 2, showing both the CNT channel region and the various source/drain contacts. The scanning electron microscope (SEM) image of a representative set of CNT-TFTs in the Ag bottom-contact design is given in Figure 2a. The SEM image in Figure 2b and AFM image in Figure 2c show the high density of the printed CNT channels. As the print conditions can greatly affect the properties of an aerosol jet printed film, we note that the semiconducting CNT films were printed with a sheath flow rate of 40 sccm, carrier flow rate of 23 sccm and speed of 2 mm/s (Figure S1). It can be seen that the density of the CNT network is consistent and approximated to be 45 CNTs/μm^2 based on the SEM and AFM images. This density is comparable to those used in previously reported CNT-TFTs.[12,37] The optical microscope image (Figure 2d) of as-printed silver lines with a width of ~40 μm and thickness of ~0.6 μm shows good uniformity and line edges. After sintering at 150 °C for 1 h, the Ag nanoparticles were partially merged together (Figure 2e,f) to give a much smaller resistance (<20 Ω/sq). For the printed gold (Au) source/drain electrodes (Figure 2g,h), a much higher sintering

DOI: 10.1021/acsnano.6b00877
ACS Nano XXXX, XXX, XXX−XXX

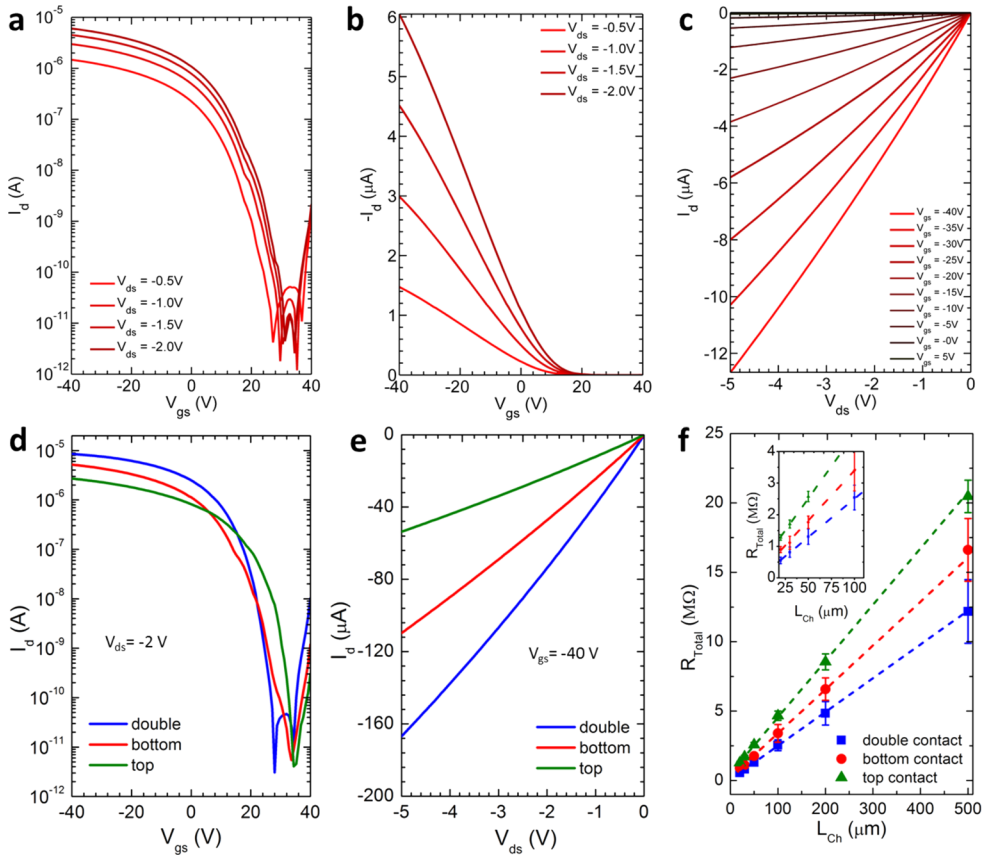

Figure 3. Characterization of printed back-gated CNT-TFTs and the impact of contact geometry with Ag contacts. (a) Subthreshold and (b) transfer characteristics (I_d–V_{gs}) of a representative, Ag bottom-contact CNT-TFT device. (c) Output (I_d–V_{ds}) characteristics from the same device with L_{ch} = 100 μm and W = 160 μm. (d) Subthreshold (I_d–V_{gs}) characteristics from representative CNT-TFTs (all having the same channel length L_{ch} = 100 μm and width W = 160 μm). (e) Output (I_d–V_{ds}) characteristics of the same devices indicating the substantial boost in on-current when moving from one contact geometry to another. (f) TLM plot of the total resistance (R_{total}) as a function of channel length (L_{ch}) for each type of Ag contact configuration. Error bars indicate the standard derivation from a set of nine tested devices.

temperature (>250 °C) was needed due to the higher melting point of Au and the necessary additive of an adhesion promoter. The SEM image in Figure 2i shows the printed metallic CNT source/drain film, which has a very dense and randomly distributed network. It is noted that in order to obtain these films of metallic CNTs with sufficient density and thus low resistivity, multiple printing passes (>10) were essential. Details on the relationship between resistivity and the number of passes for the metallic CNTs are given in the Supporting Information (Figure S2). The TLM structures used for all CNT-TFTs in this work have channel lengths (L_{ch}) of 20, 30, 50, 100, 200, and 500 μm. It should be noted that the ink properties, carrier flow rate, sheath flow rate, nozzle diameter, stage speed, and platen temperature were the main parameters adjusted for the optimization of each printed layer. The printing details for each layer/material are summarized in the Methods section.

As anticipated for CNT-TFTs that rely on percolation transport through the channel, I_{ON} increases while the I_{ON}/I_{OFF} ratio becomes smaller with decreasing channel length (Figure S3). Electrical characteristics of a representative device with Ag bottom contacts and a channel length of L_{ch} = 100 μm and channel width of W = 160 μm are given in Figure 3. It can be seen from the subthreshold characteristics (Figure 3a) that the transistor exhibits excellent on/off current ratio that is consistent at various drain-source voltages (V_{ds}). As shown in Figure S4, the printed CNT-TFTs demonstrate a relatively large hysteresis between the forward and reverse sweep, which is attributed to charge trapping at the CNT-SiO_2 interface along with adsorbed water molecules in CNT films.[38,39] On-state performance of the device (Figure 3b,c) includes an on-current at V_{ds} = −2.0 V and V_{gs} = −40 V of 6.05 μA, which corresponds to a current density of 37.8 μA/mm. The I_{ON}/I_{OFF} of the device is approximately 10^6, which is consistent with other printed CNT-TFT devices (Figure S5).

Field-effect mobility for these CNT-TFTs was calculated using the following expression: $\mu = (L_{ch}g_m)/(WC_{ox}V_{ds})$, where L_{ch} and W are the device channel length and width, respectively, g_m is the peak transconductance, V_{ds} = −2 V, and C_{ox} is the gate capacitance per unit area and was calculated by a modified parallel-plate model ($C_{ox} = \varepsilon_0\varepsilon_{ox}/t_{0x}$) as discussed in previous work.[40] On the basis of the peak transconductance extracted from the transfer curves in Figure 3b, the device mobility is 2.19 $cm^2/(V{\cdot}s)$, which is on par with other CNT-TFTs that have printed source/drain contacts and CNT channels.[25−27] It is noted that the modified parallel-plate model for determining the capacitance is likely an overestimation of the actual gate capacitance value for the CNT network devices. Thus, the calculated mobility value is a lower bound. A more rigorous and sophisticated model to calculate the capacitance is $C_{ox} = D/\{C_Q^{-1} + \ln[\sinh(2\pi Dt_{ox})/\pi RD]/(2\pi\varepsilon_0\varepsilon_{ox})\}$,[41] where C_Q is the quantum capacitance of a single CNT, D is the nanotube

DOI: 10.1021/acsnano.6b00877
ACS Nano XXXX, XXX, XXX−XXX

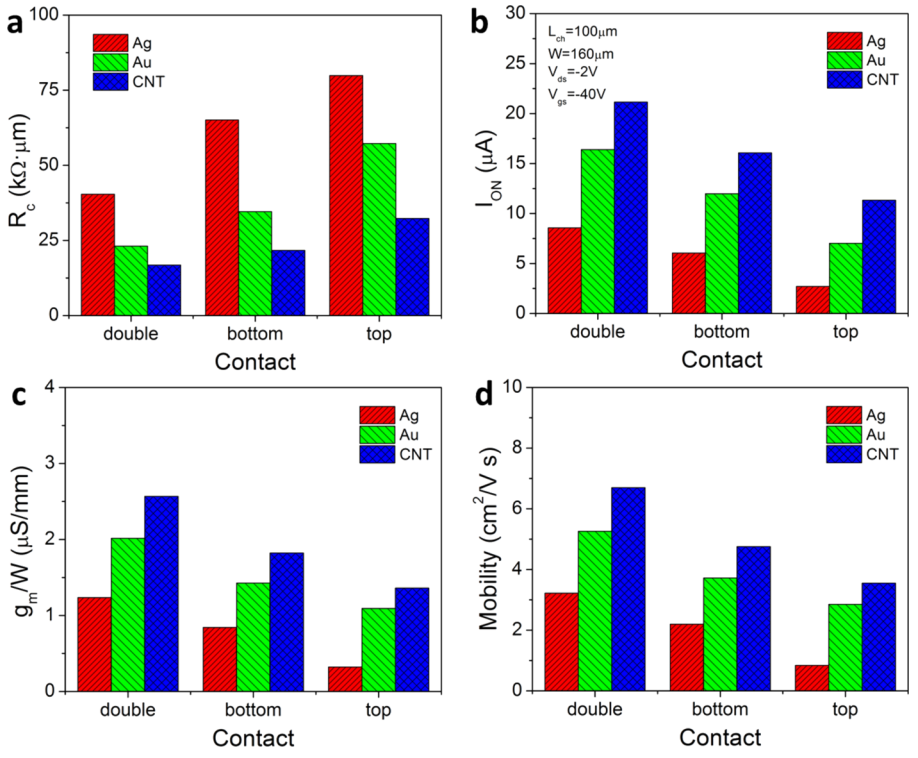

Figure 4. Comparison of key performance metrics from printed CNT-TFTs having different printed electrode materials (Ag, Au, and metallic CNT) and contact geometries (top, bottom, and double). Average (a) contact resistance, (b) I_{ON}, (c) peak transconductance g_m, and (d) mobility of the CNT-TFTs with channel length L_{ch} = 100 μm and channel width W = 160 μm.

density, R is the average diameter of the CNTs, and t_{ox} = 90 nm is the thickness of SiO_2. This gives C_{ox} = 3.56 × 10^{-8} F/cm^2, and the mobility based on this value is 2.37 cm^2/(V·s), which is similar to the one calculated by the modified parallel-plate model. This similarity agrees with the previous results reported in literature.[41] As discussed below, we were able to extract the contact resistance for these CNT-TFTs, and thus we also determined the intrinsic mobility for the CNT thin-film channel, which was found to be, on average, 3.41 cm^2/(V·s). More information about characterization (I_{on} and on/off ratio, *etc.*) of the devices with printed Ag contacts in the various geometries and at different channel lengths, as well as details for the Au and metallic CNT contacted devices, can be found in Figure S6 in the Supporting Information.

Comparison of the performance of the printed CNT-TFTs with Ag source/drain electrodes in the three different contact configurations (top, bottom, and double contacts) is also given in Figure 3. All of the devices in Figures 3d,e have the same channel length and width; hence, these representative curves offer a perspective of how the contact geometry directly affects the device performance. The off-state of the representative devices is essentially consistent, with only small variation in threshold voltage and subthreshold swing. The on-state, however, is shown to change quite dramatically between the different geometries. The initial hypothesis that the double-contact geometry would yield the best on-state performance by providing an increase in the metallic contact interfacial area to the CNTs is indeed verified by the data for Ag contacts in Figure 3d,e. It is further intriguing that there is a sizable difference between the top- and bottom-contact geometries. Historically, top contacts have been favored as they provide a more complete wrapping coverage of the CNTs.[42−44] These results reveal that the bottom contacts were able to boost the on-current by nearly a factor of 2 compared to the top contacts, a significant finding considering that the choice between one contact arrangement and the other requires no difference in overall process steps.

For further comparison of these different contact geometries, the contact resistance was extracted using the TLM structures with channel lengths ranging from 20 to 500 μm. As given in Figure 3f, the total resistance (R_{total}) is plotted as a function of channel length (L_{ch}) for each of the Ag contact geometries. R_{total} for the CNT-TFTs is $R_{total} = 2R_c + R_{ch}$, where R_{ch} is device channel resistance, and $2R_c$ is the contact resistance from the source and drain electrodes. Therefore, the contact resistance between channel and electrodes, $2R_c$, can be extracted from the intercept of the linear fit to the TLM plot and the sheet resistance of the channel is related to the slope of the linear fit.[45] The total resistance for the TLM plots in this work was taken in the on-state at V_{ds} = −0.5 V. The average extracted sheet resistance of the channel film is approximately 4.6 MΩ/sq. The extracted R_c for the top-, bottom-, and double-contact geometries with Ag are 79.9, 65.1, and 40.4 kΩ·μm, respectively. In this case, the double-contact geometry reduces the contact resistance between the printed Ag electrodes and the semiconducting CNT channel by ∼38% compared to bottom contacts and ∼49% compared to top contacts, a significant performance enhancement for CNT-TFTs. Compared to the top contact configuration, the reduction in contact resistance by using bottom or double contacts is primarily attributed to an increased contact area between the CNT thin film and the contacts. This is an especially important point with regards to the bottom contacts yielding better performance than top contacts—a rather unanticipated result when compared to most previous devices that used lithographically patterned (rather than printed) contacts. In the case of the Ag

DOI: 10.1021/acsnano.6b00877
ACS Nano XXXX, XXX, XXX−XXX

Table 1. Comparison of Performance Metrics for CNT-TFTs with Printed CNT Channel and Printed Electrodes[a]

ref	process method	contact material	contact geometry	L_{ch} (μm)	V_{ds} (V)	I_{ON} (μA/mm)	R_c (k$\Omega\cdot\mu$m)	μ (cm^2/(V s))
this work	aerosol jet	Ag	double	100	−2	53.6	40.4	3.2
this work	aerosol jet	Au	double	100	−2	102.5	23.1	5.3
this work	aerosol jet	CNT	double	155	−2	88.12	16.8	6.7
7	gravure	Ag	top	85	−5	29	-	8
24	screen print	Ag	top	105	−1	4.1	-	7.7
27	inkjet	CNT	bottom	700	−1	0.11	25	1.6−4.2
50	CVD/transfer	CNT	top	10	−0.1	0.46	-	3−20

[a]If values were not explicitly provided in the manuscripts, then they were approximated from the given data and $I-V$ curves. Metrics for devices from this work are averages of 9 CNT-TFTs.

contacts, after curing they form smooth nanoparticle grains on the order of 20−80 nm in diameter (see Figure 3f). When the semiconducting CNTs (~1 nm in diameter) are printed onto these amalgamated Ag nanoparticles, they are able to coat the smooth surfaces, including interstitially between the nanoparticles, yielding a relatively large contact area between the Ag and CNTs. In the case of the top contacts; however, the cured Ag nanoparticles are simply settled on top of the very thin film of CNTs, leading to a smaller contact area based on the many gaps between Ag nanoparticles, hence, a R_c from bottom contacts that is a nearly 20% reduction from top contacts. This same principle applies to printed Au electrodes with an even more dramatic ~40% reduction in R_c for the bottom contacts compared to the top contacts (discussed below). The semiconducting CNT film thickness may also impact the contact resistance and is worth further investigation in future work.

The same three contact geometries were studied for printed Au nanoparticle electrodes as well as printed metallic CNT electrodes, with corresponding extraction of contact resistance. The sheet resistance of Au and metallic CNT films were ~8 and ~390 Ω/sq, respectively, when measured after the curing process. A summary of the contact resistance from these printed contacts in the different configurations is given in Figure 4a. For the Au electrodes, the contact resistances are 57.3, 34.6, and 23.1 k$\Omega\cdot\mu$m, for top-, bottom-, and double-contacts, respectively. While the metallic CNT electrodes yielded R_c of 32.3, 21.7m, and 16.8 k$\Omega\cdot\mu$m for top, bottom, and double contacts, respectively. For all three of the electrode materials, the top contacts generate the highest contact resistance while double contacts exhibit the lowest. Interestingly, the metallic CNT electrodes resulted in the lowest contact resistance overall, which is attributed to the unique structure and electronic properties of the metallic CNTs.[46,47] For one, the high aspect ratio of the CNTs results in a more focused electric field at the nanotube−nanotube junctions, thus thinning the Schottky barrier.[48] Additionally, compared with Ag and Au, the surface dipole barrier of metallic CNTs is much lower, leading to more effective carrier injection.[46] Finally, the similar nanometer-scale size and overall malleability of the metallic CNT thin-film contacts is postulated to provide a higher interfacial contact area to the similarly malleable thin film of semiconducting CNTs; the metallic CNTs effectively interweaving with the semiconducting CNTs rather than just lying on top or bottom (or both) as with the metal nanoparticle contacts.

With the improvement at the contact interface between the thin-film CNT channel and printed electrodes, it can be seen from Figure 4b that the on-state currents for double contacts were much larger compared with only bottom or top contacts for all three kinds of electrodes, evidence for the dominant role that contact resistance plays in determining the performance of CNT-TFTs. In addition, the average peak transconductance (Figure 4c) and average mobility (Figure 4d) exhibited a similar trend when comparing the contact geometries, indicating improved overall performance for double contacts with respect to all key metrics.

To compare the performance of the CNT-TFTs with printed double contacts in this work to printed CNT-TFTs in the literature, a summary of key metrics is given in Table 1. All devices in the table have contacts that were printed, albeit using diverse printing approaches. Note the substantially higher on-current from the double-contact devices compared to previous studies that used the same contact materials.[7,27,49−51] It is found that all of the fully printed CNT-TFTs from a variety of printing methods (gravure printing, screen printing, inkjet printing and transfer printing) exhibited mobilities within a fairly tight distribution between 3 and 10 cm^2/(V s). The only referenced work to provide an extraction of contact resistance is the all-nanotube TFT with bottom contacts from inkjet printing (R_c ~ 25 k$\Omega\cdot\mu$m)[27] and the aerosol jet printed CNT-TFTs with double contacts in this work have a lower contact resistance (~16.8 k$\Omega\cdot\mu$m). The on-current difference between these two all-nanotube TFTs shows a more dramatic difference with the double-contact device having over 2 orders of magnitude higher current than the inkjet printed device; however, this could largely be attributed to the much longer channel length for the inkjet printed device (700 *vs* 155 μm for the double-contact device). Ultimately, this comparison among the few other reports on printed contacts to printed CNT thin films gives clear evidence of the need for more studies on contact effects and efforts like those reported in this work that seek to minimize the impact of contacts on performance in these fully printed TFTs.

As the field of printed electronics is one with strong ties to, and potential near-term realization in, industry, it is especially important to consider not only the scientifically best materials/approach based on performance, but also the impact of cost and stability. In this case, when comparing the Ag and Au electrodes, Au offers considerably better performance in the studied devices for all contact geometries, yet Au is considerably more expensive and has many issues with adhesion to different surfaces that could affect its utility as a printed electrode material. From a cost standpoint, the metallic CNT electrodes are somewhat comparable to the Ag and offer the lowest contact resistance. Yet, in spite of their low contact resistance to the semiconducting CNTs, the metallic CNT electrodes exhibited the worst conductivity of the three materials, which could have adverse effects on the stability of printed circuits if the printed metallic CNTs are used for more

DOI: 10.1021/acsnano.6b00877
ACS Nano XXXX, XXX, XXX−XXX

than just the contact regions of TFTs. Another important aspect of the cost for the metallic CNT electrodes is that they require multiple printing passes to reach an acceptable conductivity (CNT film density), which is time-consuming and thus costly in terms of throughput. A final point regarding the Au ink is that it requires sintering at much higher temperature (>250 °C), which is not suitable for most available substrates (*e.g.*, Kapton, PET, and other polymers) for flexible electronics. Hence, there are several trade-offs that must be considered when determining the most optimal printed electrode material for use in printed electronics applications.

CONCLUSIONS

In summary, we have shown that the most favorable simple contact geometry for fully printed CNT-TFTs is to have the metal contact below the printed CNT thin film channel rather than above or on top of the channel. Meanwhile, employing a combination of these bottom and top contacts to form a double-contact structure was shown to further lower contact resistance and boost CNT-TFT performance for all three printed contact materials that were studied: Ag, Au, and metallic CNTs. The metallic CNTs proved to be the best overall material for enhancing performance in the fully printed CNT-TFTs. The bottom contacts were able to boost the on-current by up to 50% compared to the top contacts, a powerful result for advising all future work on CNT-TFTs from any electrode material. These findings for the contact resistance of printed CNT-based transistors can help minimize the impact of contacts on the performance of nanomaterial-based devices and guide further development of printed nanomaterial electronics.

METHODS

Substrate Cleaning. The silicon wafers were rinsed with deionized (DI) water for 1 min, and further sonicated in acetone and isopropyl alcohol (IPA) for 10 min each (25 °C) and blown dry with N_2 gas. The wafers were subsequently subjected to 3 min of oxygen (O_2) plasma (Emitech K-1050X) at 100 W under low vacuum (0.6 Torr).[52]

Functionalization of Si Wafers. Prior to CNT channel printing, the cleaned wafer was immersed into poly-L-lysine (PLL) solution (0.1% w/v in water; Sigma-Aldrich) for 5 min to functionalize the SiO_2 surface for increasing the adhesion between printed CNT films and substrate.[1,37] The functionalized wafer was then rinsed with DI water to remove the unattached monomers, and blown dry thoroughly using N_2 gas.[37]

Printing CNT Channels. The semiconducting CNT ink (IsoSol-S100) with a purity of 99.9% semiconducting single-walled CNT and a concentration of 0.05 mg/mL was purchased from Nanointegris, Inc., Canada. It was further diluted with toluene to 0.01 mg/mL for aerosol jet printing by an AJ-300 aerosol jet printer (Optomec, Inc.), followed by 30 min ultrasonication to eliminate the aggregation of CNTs formed in the dilution process. The average length of the CNTs is about 1 μm. The as-prepared CNT ink was printed using a 150 μm diameter nozzle, and the sheath gas and carrier gas flow rates were set to be 40 and 23 sccm, respectively. The printing speed was fixed at 2 mm/s. The water bath for ink vials was kept at 20 °C. All printing was carried out in air at room temperature while the platen was maintained at 50 °C to accelerate ink drying.

Printing Ag Electrodes. The Ag ink (Ag40X, UT Dots, Inc.) contained 40 wt % Ag nanoparticles, with particle diameters ~20 nm, dispersed in a solvent mixture of xylene and terpineol (9:1 by volume). The prepared ink was printed on SiO_2/Si substrates. A 100 μm diameter nozzle was used for printing, and the flow rates of sheath gas and carrier gas were set to 25 and 15 sccm, respectively. The temperature of chilling water bath was kept at 15 °C and platen temperature was set to 60 °C. The printed samples were further sintered at 150 °C in air for 60 min in an oven (MDL 281, Fisher Scientific Co.) to enhance the conductivity.

Printing Au Electrodes. The Au ink (UTD-Au25, UT Dots, Inc.) contained 25 wt % Au nanoparticles, and was dispersed in a proprietary mixture solvent. The prepared ink was printed on SiO_2/Si substrates. A proprietary adhesion promoter (BOL from UT Dots, Inc.) was added into the Au ink to increase the adhesion strength of Au on the SiO_2. A 100 μm diameter nozzle was used for printing, and the flow rates of sheath gas and carrier gas were set to 25 and 20 sccm, respectively. Platen temperature was maintained at 80 °C, while the temperature of the chilling water bath was kept at 20 °C. The printed samples were further sintered at 280 °C in air for 1−2 h in an oven.

Printing Metallic CNT Electrodes. The P3-SWNT was purchased from Carbon Solution, Inc.. The as-received P3-SWNT powder was dispersed in DI water followed by 2 h ultrasonication to form a 0.5 mg/mL solution. The prepared ink was printed for the source and drain electrodes on SiO_2/Si substrates by the AJ-300 printer. A 150 μm diameter nozzle was used for printing, and the flow rates of sheath gas and carrier gas were set to 25 and 15 sccm, respectively, with a printing speed of 1 mm/s. To ensure a satisfactory conductivity, multiple printing passes (>5) were necessary. The water bath was kept at 25 °C and platen temperature was 30 °C. The printed samples were further sintered at 100 °C in air for 30 min in an oven.

Characterization of Printed Devices. Optical images of devices were taken by a Zeiss Axio Lab microscope configured with 2.5× to 100× objective lenses and a digital camera for image capture and analysis. SEM images of printing patterns and devices were acquired with FEI XL30 (SEM-FEG) with varied magnifications and beam conditions. AFM images of nanotubes were taken with a Dimension 3000 instrument in tapping mode.

Device Fabrication and Testing. The CNT-TFTs for the TLM measurement were printed with the AJ-300 printer with the specified parameters. For each set of devices, six different channel lengths were used: 20, 30, 50, 100, 200, and 500 μm. In printing CNT-TFTs with top-contacts, CNT channels were first printed and then followed by printing source/drain electrodes; in contrast, for CNT-TFTs with bottom contacts, source/drain electrodes were first printed on the cleaned SiO_2/Si wafers, followed by printing CNT channels on top of the source/drain electrodes, as shown in Figure 1. To fabricate the CNT-TFTs with double-contacts, another layer of contact electrodes was further printed on the bottom-contact CNT-TFTs to form a sandwich structure. After CNT channel printing, the samples were rinsed with solvent to remove residual surfactant. Electrical characterization of the printed transistors was carried out in air using a Lakeshore probe station (Lakeshore CRX-6.5K) along with an Agilent B-1500 Semiconductor Parameter Analyzer. The sheet resistance was measured with four probe methods using a Keithley 2400 and 236 source measuring units.

ASSOCIATED CONTENT

Supporting Information

The Supporting Information is available free of charge on the ACS Publications website at DOI: 10.1021/acsnano.6b00877.

Characterization of printed CNT film morphology under different printing conditions, resistance data from printed metallic CNT films, electrical data for printed CNT-TFTs using Ag contacts of various geometries, hysteresis and distribution present in CNT-TFTs, and electrical data for printed CNT-TFTs using Au and metallic CNT contacts of various types (PDF)

AUTHOR INFORMATION

Corresponding Author

*E-mail: aaron.franklin@duke.edu.

Notes

The authors declare no competing financial interest.

DOI: 10.1021/acsnano.6b00877
ACS Nano XXXX, XXX, XXX−XXX

ACKNOWLEDGMENTS

We acknowledge Y. Fang for help with experimental measurement and data analysis. We also thank D. Frisbie from the University of Minnesota and M. Renn from Optomec, Inc., for discussions on CNT aerosol jet printing. The work was supported by funding from Fetch Automotive Design Group, LLC.

REFERENCES

(1) Wang, C.; Zhang, J.; Ryu, K.; Badmaev, A.; De Arco, L. G.; Zhou, C. Wafer-Scale Fabrication of Separated Carbon Nanotube Thin-Film Transistors for Display Applications. *Nano Lett.* **2009**, *9*, 4285−4291.

(2) Cao, Q.; Kim, H.; Pimparkar, N.; Kulkarni, J. P.; Wang, C.; Shim, M.; Roy, K.; Alam, M. A.; Rogers, J. A. Medium-Scale Carbon Nanotube Thin-Film Integrated Circuits on Flexible Plastic Substrates. *Nature* **2008**, *454*, 495−500.

(3) Timmermans, M. Y.; Estrada, D.; Nasibulin, A. G.; Wood, J. D.; Behnam, A.; Sun, D. M.; Ohno, Y.; Lyding, J. W.; Hassanien, A.; Pop, E.; Kauppinen, E. I. Effect of Carbon Nanotube Network Morphology on Thin Film Transistor Performance. *Nano Res.* **2012**, *5*, 307−319.

(4) Sun, D.; Timmermans, M. Y.; Tian, Y.; Nasibulin, A. G.; Kauppinen, E. I.; Kishimoto, S.; Mizutani, T.; Ohno, Y. Flexible High-Performance Carbon Nanotube Integrated Circuits. *Nat. Nanotechnol.* **2011**, *6*, 156−161.

(5) Jang, K.-I.; Chung, H. U.; Xu, S.; Lee, C. H.; Luan, H.; Jeong, J.; Cheng, H.; Kim, G.-T.; Han, S. Y.; Lee, J. W.; Kim, J.; Cho, M.; Miao, F.; Yang, Y.; Jung, H. N.; Flavin, M.; Liu, H.; Kong, G. W.; Yu, K. J.; Rhee, S. I.; et al. Soft Network Composite Materials with Deterministic and Bio-Inspired Designs. *Nat. Commun.* **2015**, *6*, 6566.

(6) Chortos, A.; Koleilat, G. I.; Pfattner, R.; Kong, D.; Lin, P.; Nur, R.; Lei, T.; Wang, H.; Liu, N.; Lai, Y.-C.; Kim, M. G.; Chung, J. W.; Lee, S.; Bao, Z. Mechanically Durable and Highly Stretchable Transistors Employing Carbon Nanotube Semiconductor and Electrodes. *Adv. Mater.* **2015**, DOI: 10.1002/adma.201501828.

(7) Lau, P. H.; Takei, K.; Wang, C.; Ju, Y.; Kim, J.; Yu, Z.; Takahashi, T.; Cho, G.; Javey, A. Fully Printed, High Performance Carbon Nanotube Thin-Film Transistors on Flexible Substrates. *Nano Lett.* **2013**, *13*, 3864−3869.

(8) Franklin, A. D. Nanomaterials in Transistors: From High-Performance to Thin-Film Applications. *Science* **2015**, *349*, aab2750.

(9) Hur, S. H.; Yoon, M. H.; Gaur, A.; Shim, M.; Facchetti, A.; Marks, T. J.; Rogers, J. A. Organic Nanodielectrics for Low Voltage Carbon Nanotube Thin Film Transistors and Complementary Logic Gates. *J. Am. Chem. Soc.* **2005**, *127*, 13808−13809.

(10) Zhou, Y.; Gaur, A.; Hur, S.-H.; Kocabas, C.; Meitl, M. a; Shim, M.; Rogers, J. A. P-Channel, N-Channel Thin Film Transistors and P−n Diodes Based on Single Wall Carbon Nanotube Networks. *Nano Lett.* **2004**, *4*, 2031−2035.

(11) Kang, H.; Park, H.; Park, Y.; Jung, M.; Kim, B. C.; Wallace, G.; Cho, G. Fully Roll-to-Roll Gravure Printable Wireless (13.56 MHz) Sensor-Signage Tags for Smart Packaging. *Sci. Rep.* **2014**, *4*, 5387.

(12) Wang, C.; Takei, K.; Takahashi, T.; Javey, A. Carbon Nanotube Electronics -Moving Forward. *Chem. Soc. Rev.* **2013**, *42*, 2592−2609.

(13) Tu, X.; Manohar, S.; Jagota, A.; Zheng, M. DNA Sequence Motifs for Structure-Specific Recognition and Separation of Carbon Nanotubes. *Nature* **2009**, *460*, 250−253.

(14) Lee, H. W.; Yoon, Y.; Park, S.; Oh, J. H.; Hong, S.; Liyanage, L. S.; Wang, H.; Morishita, S.; Patil, N.; Park, Y. J.; Park, J. J.; Spakowitz, A.; Galli, G.; Gygi, F.; Wong, P. H.-S.; Tok, J. B.-H.; Kim, J. M.; Bao, Z. Selective Dispersion of High Purity Semiconducting Single-Walled Carbon Nanotubes with Regioregular poly(3-Alkylthiophene)s. *Nat. Commun.* **2011**, *2*, 541.

(15) Green, A. A.; Hersam, M. C. Nearly Single-Chirality Single-Walled Carbon Nanotubes Produced via Orthogonal Iterative Density Gradient Ultracentrifugation. *Adv. Mater.* **2011**, *23*, 2185−2190.

(16) Tulevski, G. S.; Franklin, A. D.; Afzali, A. High Purity Isolation and Quantification of Semiconducting Carbon Nanotubes via Column Chromatography. *ACS Nano* **2013**, *7*, 2971−2976.

(17) Cao, Q.; Han, S.-J.; Tulevski, G. S.; Franklin, A. D.; Haensch, W. Evaluation of Field-Effect Mobility and Contact Resistance of Transistors That Use Solution-Processed Single-Walled Carbon Nanotubes. *ACS Nano* **2012**, *6*, 6471−6477.

(18) Tersoff, J. Contact Resistance of Carbon Nanotubes. *Appl. Phys. Lett.* **1999**, *74*, 2122−2124.

(19) Ha, M.; Seo, J.-W. T. W. T.; Prabhumirashi, P. L.; Zhang, W.; Geier, M. L.; Renn, M. J.; Kim, C. H.; Hersam, M. C.; Frisbie, C. D. Aerosol Jet Printed, Low Voltage, Electrolyte Gated Carbon Nanotube Ring Oscillators with Sub-5 μs Stage Delays. *Nano Lett.* **2013**, *13*, 954−960.

(20) Sirringhaus, H.; Kawase, T.; Friend, R. H.; Shimoda, T.; Inbasekaran, M.; Wu, W.; Woo, E. P. High-Resolution Inkjet Printing of All-Polymer Transistor Circuits. *Science* **2000**, *290*, 2123−2126.

(21) Franklin, A. D.; Chen, Z. Length Scaling of Carbon Nanotube Transistors. *Nat. Nanotechnol.* **2010**, *5*, 858−862.

(22) Javey, A.; Guo, J.; Wang, Q.; Lundstrom, M.; Dai, H. Ballistic Carbon Nanotube Field-Effect Transistors. *Nature* **2003**, *424*, 654−657.

(23) Wu, Y.; Li, Y.; Ong, B. S.; Liu, P.; Gardner, S.; Chiang, B. High-Performance Organic Thin-Film Transistors with Solution-Printed Gold Contacts. *Adv. Mater.* **2005**, *17*, 184−187.

(24) Cao, X.; Chen, H.; Gu, X.; Liu, B.; Wang, W.; Cao, Y.; Wu, F.; Zhou, C. Screen Printing as a Scalable and Low-Cost Approach for Rigid and Flexible Thin-Film Transistors Using Separated Carbon Nanotubes. *ACS Nano* **2014**, *8*, 12769−12776.

(25) Park, S.; Vosguerichian, M.; Bao, Z. A Review of Fabrication and Applications of Carbon Nanotube Film-Based Flexible Electronics. *Nanoscale* **2013**, *5*, 1727−1752.

(26) Beecher, P.; Servati, P.; Rozhin, a.; Colli, A.; Scardaci, V.; Pisana, S.; Hasan, T.; Flewitt, a. J.; Robertson, J.; Hsieh, G. W.; Li, F. M.; Nathan, A.; Ferrari, A. C.; Milne, W. I. Ink-Jet Printing of Carbon Nanotube Thin Film Transistors. *J. Appl. Phys.* **2007**, *102*, 043710.

(27) Okimoto, H.; Takenobu, T.; Yanagi, K.; Miyata, Y.; Shimotani, H.; Kataura, H.; Iwasa, Y. Tunable Carbon Nanotube Thin-Film Transistors Produced Exclusively via Inkjet Printing. *Adv. Mater.* **2010**, *22*, 3981−3986.

(28) Ha, M.; Xia, Y.; Green, A. a; Zhang, W.; Renn, M. J.; Kim, C. H.; Hersam, M. C.; Frisbie, C. D. Printed, Sub-3V Digital Circuits on Plastic from Aqueous Carbon Nanotube Inks. *ACS Nano* **2010**, *4*, 4388−4395.

(29) Hong, K.; Kim, S. H.; Mahajan, A.; Frisbie, C. D. Aerosol Jet Printed P- and N-Type Electrolyte-Gated Transistors with a Variety of Electrode Materials: Exploring Practical Routes to Printed Electronics. *ACS Appl. Mater. Interfaces* **2014**, *6*, 18704.

(30) Ha, M.; Zhang, W.; Braga, D.; Renn, M. J.; Kim, C. H.; Frisbie, C. D. Aerosol-Jet-Printed, 1 V H-Bridge Drive Circuit on Plastic with Integrated Electrochromic Pixel. *ACS Appl. Mater. Interfaces* **2013**, *5*, 13198−13206.

(31) Hong, K.; Kim, Y. H.; Kim, S. H.; Xie, W.; Xu, W. D.; Kim, C. H.; Frisbie, C. D. Aerosol Jet Printed, Sub-2 V Complementary Circuits Constructed from P- and N-Type Electrolyte Gated Transistors. *Adv. Mater.* **2014**, *26*, 7131.

(32) Kang, S. J.; Kocabas, C.; Ozel, T.; Shim, M.; Pimparkar, N.; Alam, M. a; Rotkin, S. V.; Rogers, J. A. High-Performance Electronics Using Dense, Perfectly Aligned Arrays of Single-Walled Carbon Nanotubes. *Nat. Nanotechnol.* **2007**, *2*, 230−236.

(33) Stokes, P.; Khondaker, S. I. High Quality Solution Processed Carbon Nanotube Transistors Assembled by Dielectrophoresis. *Appl. Phys. Lett.* **2010**, *96*, 083110.

(34) Wang, C.; Chien, J.-C.; Takei, K.; Takahashi, T.; Nah, J.; Niknejad, A. M.; Javey, A. Extremely Bendable, High Performance Integrated Circuits Using Semiconducting Carbon Nanotube Networks for Digital, Analog, and Radio-Frequency Applications. *Nano Lett.* **2012**, *12*, 1527−1533.

(35) Takahashi, T.; Takei, K.; Gillies, A. G.; Fearing, R. S.; Javey, A. Carbon Nanotube Active-Matrix Backplanes for Conformal Electronics and Sensors. *Nano Lett.* **2011**, *11*, 5408−5413.

DOI: 10.1021/acsnano.6b00877
ACS Nano XXXX, XXX, XXX−XXX

(36) Li, S.; Park, J. G.; Wang, S.; Liang, R.; Zhang, C.; Wang, B. Working Mechanisms of Strain Sensors Utilizing Aligned Carbon Nanotube Network and Aerosol Jet Printed Electrodes. *Carbon* **2014**, *73*, 303−309.
(37) Zhang, J.; Fu, Y.; Wang, C.; Chen, P.-C. C.; Liu, Z.; Wei, W.; Wu, C.; Thompson, M. E.; Zhou, C. Separated Carbon Nanotube Macroelectronics for Active Matrix Organic Light-Emitting Diode Displays. *Nano Lett.* **2011**, *11*, 4852−4858.
(38) Kim, W.; Javey, A.; Vermesh, O.; Wang, Q.; Li, Y.; Dai, H. Hysteresis Caused by Water Molecules in Carbon Nanotube Field-Effect Transistors. *Nano Lett.* **2003**, *3*, 193−198.
(39) Jin, S. H.; Islam, A. E.; Kim, T.-i.; Kim, J. H.; Alam, M. a.; Rogers, J. a. Sources of Hysteresis in Carbon Nanotube Field-Effect Transistors and Their Elimination via Methylsiloxane Encapsulants and Optimized Growth Procedures. *Adv. Funct. Mater.* **2012**, *22*, 2276−2284.
(40) Cao, Q.; Xia, M.; Kocabas, C.; Shim, M.; Rogers, J. A.; Rotkin, S. V. Gate Capacitance Coupling of Singled-Walled Carbon Nanotube Thin-Film Transistors. *Appl. Phys. Lett.* **2007**, *90*, 023516.
(41) Chen, P.; Fu, Y.; Aminirad, R.; Wang, C.; Zhang, J.; Wang, K.; Galatsis, K.; Zhou, C. Fully Printed Separated Carbon Nanotube Thin Film Transistor Circuits and Its Application in Organic Light Emitting Diode Control. *Nano Lett.* **2011**, *11*, 5301−5308.
(42) Zhao, J.; Gao, Y.; Gu, W.; Wang, C.; Lin, J.; Chen, Z.; Cui, Z. Fabrication and Electrical Properties of All-Printed Carbon Nanotube Thin Film Transistors on Flexible Substrates. *J. Mater. Chem.* **2012**, *22*, 20747−20753.
(43) Aikawa, S.; Einarsson, E.; Thurakitseree, T.; Chiashi, S.; Nishikawa, E.; Maruyama, S. Deformable Transparent All-Carbon-Nanotube Transistors. *Appl. Phys. Lett.* **2012**, *100*, 9063502.
(44) Wang, C.; Takei, K.; Takahashi, T.; Javey, A. Carbon Nanotube Electronics − Moving Forward. *Chem. Soc. Rev.* **2013**, *42*, 2592−2609.
(45) Ante, F.; Kälblein, D.; Zaki, T.; Zschieschang, U.; Takimiya, K.; Ikeda, M.; Sekitani, T.; Someya, T.; Burghartz, J. N.; Kern, K.; Klauk, H. Contact Resistance and Megahertz Operation of Aggressively Scaled Organic Transistors. *Small* **2012**, *8*, 73−79.
(46) Cao, Q.; Zhu, Z.-T.; Lemaitre, M. G.; Xia, M.-G.; Shim, M.; Rogers, J. A. Transparent Flexible Organic Thin-Film Transistors That Use Printed Single-Walled Carbon Nanotube Electrodes. *Appl. Phys. Lett.* **2006**, *88*, 113511.
(47) Qi, P.; Javey, A.; Rolandi, M.; Wang, Q.; Yenilmez, E.; Dai, H. Miniature Organic Transistors with Carbon Nanotubes as Quasi-One-Dimensional Electrodes. *J. Am. Chem. Soc.* **2004**, *126*, 11774−11775.
(48) Heinze, S.; Tersoff, J.; Martel, R.; Derycke, V.; Appenzeller, J.; Avouris, P. Carbon Nanotubes as Schottky Barrier Transistors. *Phys. Rev. Lett.* **2002**, *89*, 106801.
(49) Zou, Y.; Li, Q.; Liu, J.; Jin, Y.; Qian, Q.; Jiang, K.; Fan, S. Fabrication of All-Carbon Nanotube Electronic Devices on Flexible Substrates through CVD and Transfer Methods. *Adv. Mater.* **2013**, *25*, 6050−6056.
(50) Chang, C. H.; Chien, C. H. Functionalized Single-Walled Carbon-Nanotube-Blended P3HT-Based Thin-Film Transistors with Multiwalled Carbon-Nanotube Source and Drain Electrodes. *IEEE Electron Device Lett.* **2011**, *32*, 1457−1459.
(51) Li, S.; Liu, C.; Hou, P.-X.; Sun, D.-M.; Cheng, H.-M. Enrichment of Semiconducting Single-Walled Carbon Nanotubes by Carbothermic Reaction for Use in All-Nanotube Field Effect Transistors. *ACS Nano* **2012**, *6*, 9657−9661.
(52) Luck, K. A.; Shastry, T. A.; Loser, S.; Ogien, G.; Marks, T. J.; Hersam, M. C. Improved Uniformity in High-Performance Organic Photovoltaics Enabled by (3-Aminopropyl)triethoxysilane Cathode Functionalization. *Phys. Chem. Chem. Phys.* **2013**, *15*, 20966−20972.

DOI: 10.1021/acsnano.6b00877
ACS Nano XXXX, XXX, XXX−XXX